Studies on spatial modes and the correlation anisotropy of entangled photons generated from 2D quadratic nonlinear photonic crystals

2017 J. Opt. 19 065201

(http://iopscience.iop.org/2040-8986/19/6/065201)

IOP Publishing
Journal of Optics
J. Opt. **19** (2017) 065201 (8pp)
https://doi.org/10.1088/2040-8986/aa6a61

Studies on spatial modes and the correlation anisotropy of entangled photons generated from 2D quadratic nonlinear photonic crystals

X W Luo, P Xu, C W Sun, H Jin, R J Hou, H Y Leng and S N Zhu

National Laboratory of Solid State Microstructures and College of Physics, Nanjing University, Nanjing 210093, People's Republic of China

E-mail: pingxu520@nju.edu.cn

Received 16 November 2016, revised 26 March 2017
Accepted for publication 31 March 2017
Published 28 April 2017

Abstract

Concurrent spontaneous parametric down-conversion (SPDC) processes have proved to be an appealing approach for engineering the path-entangled photonic state with designable and tunable spatial modes. In this work, we propose a general scheme to construct high-dimensional path entanglement and demonstrate the basic properties of concurrent SPDC processes from domain-engineered quadratic nonlinear photonic crystals, including the spatial modes and the photon flux, as well as the anisotropy of spatial correlation under noncollinear quasi-phase-matching geometry. The overall understanding about the performance of concurrent SPDC processes will give valuable references to the construction of compact path entanglement and the development of new types of photonic quantum technologies.

Keywords: quantum state engineering, entanglement production and manipulation, spontaneous parametric down-conversion, correlation anisotropy

(Some figures may appear in colour only in the online journal)

1. Introduction

Developing quantum light source is of essential importance to quantum fundamentals and quantum technologies [1, 2]. A conventional and well-developed method to prepare entangled photon pairs is spontaneous parametric down-conversion (SPDC) in nonlinear optical mediums. When momentum and energy conservations are satisfied in such materials, a higher-energy pump photon will split into two lower-energy photons, namely the signal and idler. Continuous efforts towards desirable quantum light source which emits bright, robust and flexible entangled states have been made in recent years from different quadratic materials. Among them, quadratic nonlinear photonic crystal (NPC) with periodically modulated nonlinearity $\chi^{(2)}$ [3, 4] is a peculiar one wherein the quasi-phase-matching (QPM) condition is fulfilled with the reciprocal vector rising from the modulated dielectric domain structure, hence the entangled property of photon pairs can be intrinsically different from those from bulk homogeneous crystals [5].

When the quadratic NPC is designed to supply multiple reciprocal vectors, several QPM parametric down-conversion processes can happen simultaneously in the single quadratic NPC [6–11]. Extending this concurrent yet classical scheme to the quantum regime, multiple reciprocal vectors in a single quadratic NPC give simultaneous excitation of several SPDC processes, i.e. concurrent SPDC processes [12–14], thus enriching the variety of entanglement as well as providing high-dimensional entangled states.

Two-photon amplitudes of down-converted photons from quadratic NPCs differ in polarization [15–19], frequency [20–23], spatial mode [13, 14, 24–27] or angular momentum [28–30], which acts as the key advantage of such crystals over the homogeneous ones, thus underlines the compact generation of various photonic states. Among those, the path-entangled state is of great interest since it has potential applications in quantum communication, quantum metrology and quantum computation as well as possible extension to high-dimensional Hilbert space and multi-photon fashion. A path-entangled state such as NOON state, W state etc is usually constructed by post-processing after the photons generated from homogeneous nonlinear crystal. In recent years, the concurrent SPDC processes in a monolithic NPC are proposed to be a direct way for generating path entanglement, however only two-dimensional NOON state is studied [12–14]. Here in this work, we for the first time propose the general method for engineering the high-dimensional path-entangled state from a single NPC based on the combinations of noncollinear concurrent QPM geometries. Meanwhile, two-photon spatial correlation in noncollinear geometry is studied. The anisotropy of spatial correlation is found to be related to the noncollinear QPM geometry as well as the pump focusing. In addition, we made a comprehensive study on the spatial modes and photon flux under typical concurrent SPDC processes. These studies give a detailed description for the spatial properties of entangled photons generated by concurrent SPDC processes, which will further shed light on the construction of compact path entanglement and the development of new types of photonic quantum technologies.

The paper is structured as follows. In section 2, single-photon properties of down-converted photons are discussed, including the spatial modes and the photon flux. Theoretical descriptions and experimental results for the anisotropic spatial correlation are introduced in section 3. After these analyses, we make a discussion about the potential application of 2D quadratic NPCs as integrated quantum light sources in section 4.

2. Single-photon properties of down-converted photons generated in 2D quadratic NPCs

2.1. The general two-photon state generated by QPM-SPDC process

For an infinitely large quadratic NPC, the periodically modulated quadratic nonlinearity can be expressed by

$$\chi^{(2)}(\vec{r}) = d_{33}\sum_{m,n} f_{m,n}\, \mathrm{e}^{-\mathrm{i}\vec{G}_{m,n}\cdot\vec{r}}, \tag{1}$$

in which $\vec{G}_{m,n}$ $(m,\ n = 0,\ \pm1,\ \pm2\cdots)$ is the reciprocal vector with corresponding Fourier coefficient $f_{m,n}$ [3]. d_{33} is used since the polarization configuration of discussed QPM-SPDC process is $e \to (e + e)$. In the following discussion and experiments all the SPDC processes are degenerate.

Taking $\chi^{(2)}(\vec{r})$ into the interaction Hamiltonian,

$$H_I = \varepsilon_0\int_V \mathrm{d}\vec{r}\chi^{(2)}(\vec{r})\{E_\mathrm{p}^{(+)}E_\mathrm{s}^{(-)}E_\mathrm{i}^{(-)}\} + \mathrm{h.\ c.}, \tag{2}$$

we obtain a general two-photon state based on the first-order perturbation theory [31],

$$|\psi\rangle = \psi_0\sum_{m,n} f_{mn}\,\delta^{(3)}(\vec{k}_\mathrm{s} + \vec{k}_\mathrm{i} + \vec{G}_{m,n} - \vec{k}_\mathrm{p})\hat{a}^\dagger(\vec{k}_\mathrm{s})\hat{a}^\dagger(\vec{k}_\mathrm{i})|0\rangle. \tag{3}$$

All the slowly varying terms and constants are absorbed into ψ_0. $\vec{k}_\mathrm{p}$, $\vec{k}_\mathrm{s}$, and $\vec{k}_\mathrm{i}$ are wave vectors of the pump, signal and idler, respectively. Here for simplicity we have assumed that the cross section of the crystal is much larger than the interaction area, so that the transverse integration range can be considered as infinite. Also the crystal length is considered to be infinite so that the single longitudinal mode approximation is satisfied. We can see from equation (3) that effective SPDC process calls for satisfaction of the phase-matching condition $\vec{k}_\mathrm{s} + \vec{k}_\mathrm{i} + \vec{G}_{m,n} - \vec{k}_\mathrm{p} = 0$.

2.2. Typical QPM geometries of concurrent SPDC processes

For a single QPM-SPDC process in which only one reciprocal vector is involved, the collinear QPM geometry is indicated by figure 1(a). In this case, the spatial forms of down-converted photons are similar with those in birefringence-phase-matching (BPM) SPDC processes. However, in two-dimensional quadratic NPCs, multiple noncollinear reciprocal vectors could be involved, resulting in rich QPM geometries. Figure 1(b) illuminates two typical QPM conditions wherein two concurrent SPDC processes take place in a hexagonal quadratic NPC. The coexisting pair of QPM geometries follow $\vec{k}_\mathrm{p} - \vec{G}_{1,0} - \vec{k}_\mathrm{s} - \vec{k}_\mathrm{i} = 0$ and $\vec{k}_\mathrm{p} - \vec{G}_{0,1} - \vec{k}_\mathrm{s} - \vec{k}_\mathrm{i} = 0$. Generally, the down-converted photons will emit as either one of conical beams with principle axis along $\vec{k}_\mathrm{p} - \vec{G}_{1,0}$ or $\vec{k}_\mathrm{p} - \vec{G}_{0,1}$. Here we illustrate two typical QPM geometries. The upper of figure 1(b) corresponds to the beam-like emission of two-photon NOON state, i.e. two photons simultaneously occupy either one of the two spatial modes. It is a two-photon maximally path-entangled state in the form of $(|20\rangle + |02\rangle)/\sqrt{2}$, while the lower one corresponds to the emission of heralded single-photon path entanglement which have been studied in [14]. The quantum states can be written as

$$|\psi\rangle = \frac{1}{2}(\hat{a}_1^{\dagger 2} + \hat{a}_2^{\dagger 2})|0\rangle \tag{4}$$

and

$$|\psi\rangle = \frac{1}{\sqrt{2}}\hat{a}_\mathrm{i}^\dagger(\hat{a}_\mathrm{s1}^\dagger + \hat{a}_\mathrm{s2}^\dagger)|0\rangle, \tag{5}$$

respectively. With the tilted reciprocal vectors, the signal and idler photons can appear from the same side of the pump even sharing the same spatial mode as sketched in the upper of figure 1(b) which differs from the BPM SPDC process.

Similarly, the down-converted photons from three concurrent SPDC processes will emit as three conical beams. Figure 1(c) describes a particular QPM geometry of three concurrent SPDC processes. Three reciprocal vectors, namely $\vec{G}_{2,0}$, $\vec{G}_{0,2}$ and $\vec{G}_{1,1}$ which are supplied by a tetragonal quadratic NPC, can provide two beam-like modes which are designed to overlap with the in-plane modes of another conical beam emission of down-converted photons at a certain temperature. QPM conditions can be written as $\vec{k}_\mathrm{s1} + \vec{k}_\mathrm{i1} + \vec{G}_{2,0} - \vec{k}_\mathrm{p} = 0$, $\vec{k}_\mathrm{s2} + \vec{k}_\mathrm{i2} + \vec{G}_{0,2} - \vec{k}_\mathrm{p} = 0$, and $\vec{k}_\mathrm{s2(1)} + \vec{k}_\mathrm{i1(2)} + \vec{G}_{1,1} - \vec{k}_\mathrm{p} = 0$. Therefore, a three-

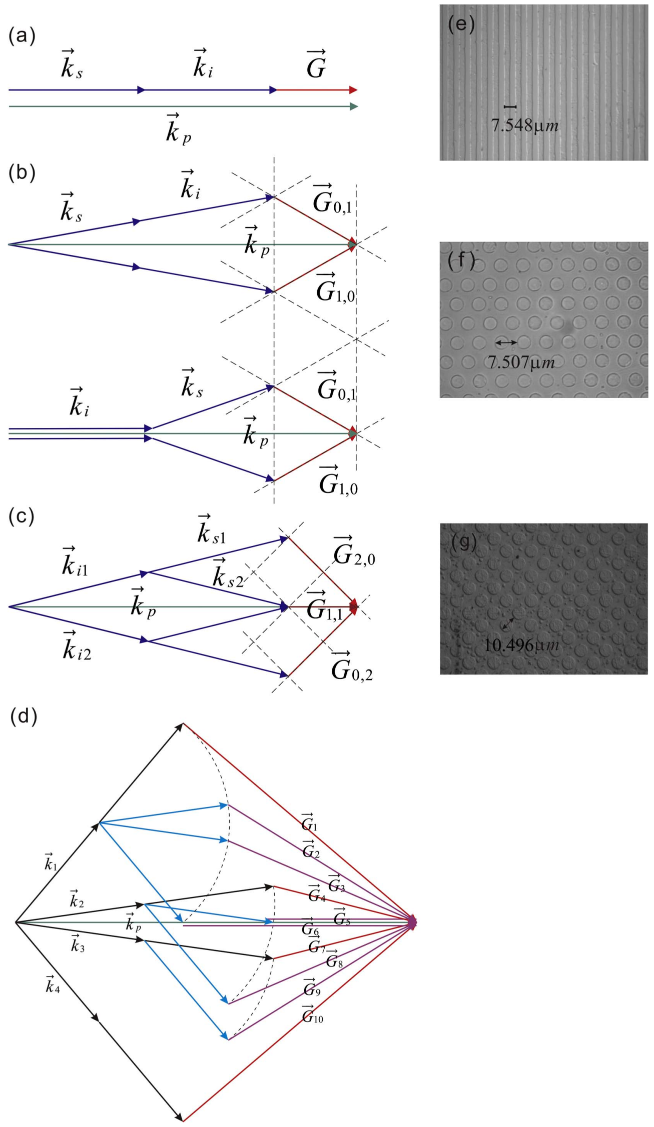

Figure 1. (a) The QPM geometry of collinear SPDC in one-dimensional PPLT crystal. (b) Two typical QPM geometries in a HPLT crystal for the generation of two-photon NOON state and single-photon path entanglement. (c) The QPM geometry of high-dimensional path-entangled state achieved in a RPLT crystal where three concurrent SPDC processes take place simultaneously. (d) The sketch of the concurrent QPM geometry of high-dimensional path-entangled state achieved in cascaded 2D poled crystal. Micrographs of the corresponding crystals: (e) 1D PPLT, (f) HPLT, and (g) RPLT.

dimensional path-entangled state

$$|\psi\rangle = \psi_0(f_{2,0}\eta_1\hat{a}_1^{\dagger 2} + f_{0,2}\eta_2\hat{a}_2^{\dagger 2} + f_{1,1}\eta_3\hat{a}_1^{\dagger}\hat{a}_2^{\dagger})|0\rangle \tag{6}$$

can be generated. $\eta_j (j = 1,\ 2,\ 3)$ are the fiber collection efficiencies for the three SPDC processes. The SPDC processes fulfilled by $\vec{G}_{2,0}$ and $\vec{G}_{0,2}$ are spatially symmetric and can be considered to be identical with $\eta_1 = \eta_2$ and $f_{2,0} = f_{0,2}$. If we let $\beta = f_{2,0}\eta_1 = f_{0,2}\eta_2$ and $\gamma = f_{1,1}\eta_3$, equation (6) can be simply written into

$$|\psi\rangle \propto \beta(|2,\ 0\rangle + |0,\ 2\rangle) + \gamma|1,\ 1\rangle. \tag{7}$$

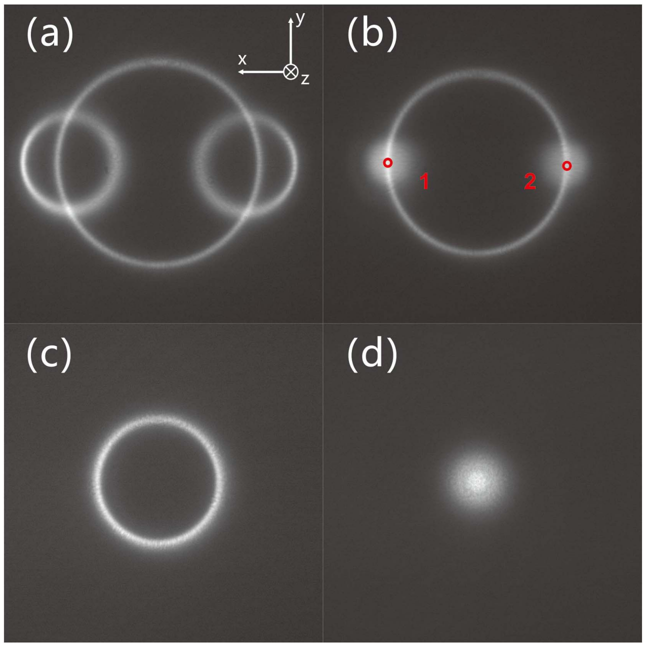

Figure 2. The experimental capture of spatial distributions of the down-converted photons generated from the RPLT crystal, which are captured at the focal plane of a convex lens when the temperature of crystal is controlled at (a) 160 °C, (b) 176 °C, (c) 205 °C, and (d) 226 °C.

Such three-dimensional path-entangled state can supply as the basis for constructing other types of path entanglement such as multi-photon path entanglement when seeded by a two-mode coherent state [12].

In general, such flexible design of reciprocal vectors provides an extensible scheme to the higher-dimensional entangled states. For example, figure 1(d) is a sketch of the QPM geometry of generating a general high-dimensional path-entangled state,

$$|\psi\rangle = \sum_{m=1}^{M} P_m|0_1 0_2 2_m\ \cdots\ 0_{M-1}0_M\rangle + \sum_{i\neq j}^{M} Q_{i,j}|0_1 0_2 1_i\ \cdots\ 1_j 0_{M-1}0_M\rangle. \tag{8}$$

This general path entangled state contains M spatial modes in total and indicating all the possibilities of two photons to be distributed into the same mode or different modes. Such concurrent SPDC process can be realized by a series of cascaded $\chi^{(2)}$–inverted structures on a single quadratic NPC wafer. This high-dimensional path-entangled state gives rise to different types of W states with controllable modes.

2.3. Experimental measurement of spatial modes of concurrent QPM-SPDC processes

The aforementioned theoretical design of concurrent SPDC processes is experimentally studied here by capturing the spatial mode of photon pairs from several types of quadratic NPCs. In our experiment, the pump laser is 532 nm, and the wavelength of degenerated down-converted photons is

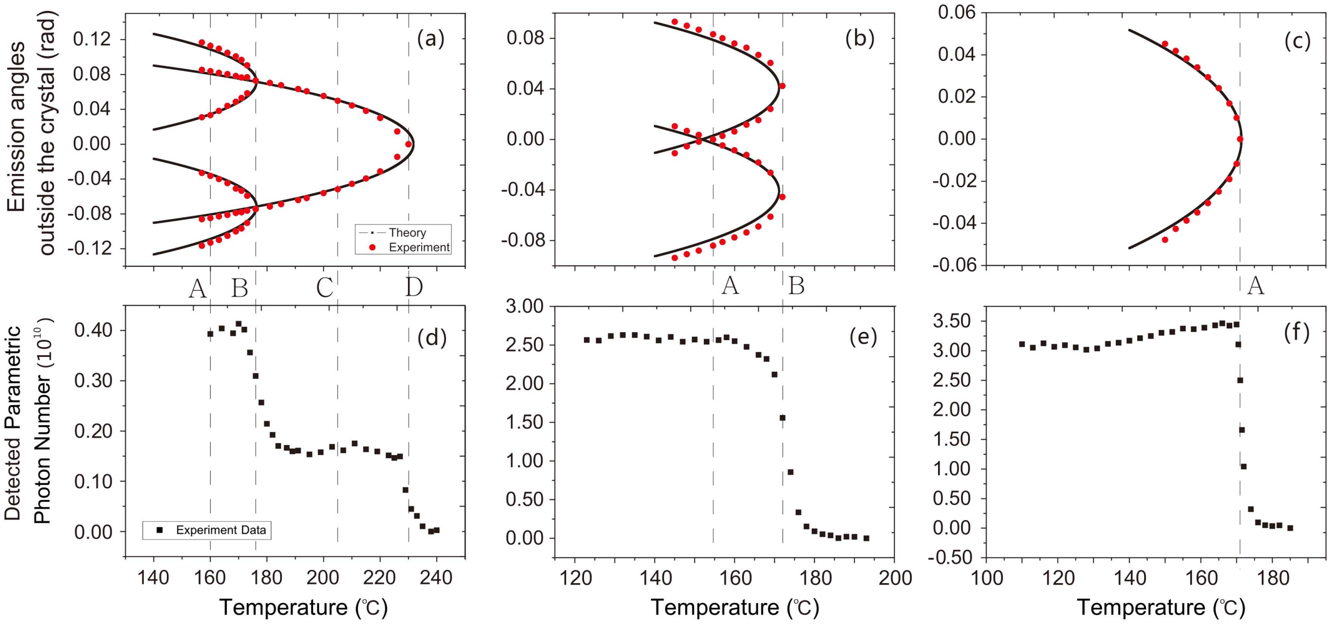

Figure 3. (a)–(c) In-plane emission angles (outside quadratic NPCs) of the down-converted photons at different temperatures in RPLT, HPLT and PPLT respectively. (d)–(f) Measured photon flux in RPLT, HPLT and PPLT respectively.

1064 nm. The polarization configuration of concurrent QPM-SPDC processes is $e \to (e + e)$ so that d_{33} is used. We design three different quadratic NPCs as shown in figure 1. The first one is one-dimensional periodically poled lithium tantalate (PPLT, see figure 1(e), the poling period is 5.248 μm), in which collinear QPM condition is fulfilled as illuminated in figure 1(a). The second quadratic NPC is a hexagonally poled lithium tantalate (HPLT, see figure 1(f), the side length of the hexagon is 7.507 μm), wherein two reciprocal vectors are involved in concurrent SPDC processes and the path-entangled states described by equations (4) and (5) can be generated. Thirdly we design a rectangularly poled lithium tantalate (RPLT, see figure 1(g), the side length of the quadrate is 10.496 μm) inside which the path-entangled state described by equation (7) is generated by three concurrent SPDC processes.

The spatial mode of photon pairs varies with the temperature since wave vectors of pump, signal and idler photons are temperature-dependent [32]. The spatial distribution of down-converted photons at different temperature is captured by a CCD (Princeton Pixis 1024B) at the Fourier plane of an $f = 50$ mm lens behind the crystal. We choose the RPLT crystal sketched by figure 1(g) as a representative because it covers most of the possible concurrent SPDC processes in 2D quadratic NPCs. Figures 2(a)–(d) show the measured spatial distribution evolution when the temperature increases. Figure 3(a) shows the quantitative information about the spatial distributions, indicating the temperature-dependence of the noncollinear emission angles in x–z plane, in which the three curves correspond to the SPDC processes supported by $\vec{G}_{2,0}$, $\vec{G}_{0,2}$ and $\vec{G}_{1,1}$, respectively. Temperature points A–D in figure 3(a) correspond to the situations of figures 2(a)–(d), respectively. At a low temperature (point A) all the SPDC processes occur, with down-converted photons emitting in three cones. When the temperature increases, the cones will shrink and at a particular temperature (point B in figure 3(a)), the spatial distribution of down-converted photons will exhibit a conical and two beam-like modes, as shown in figure 2(b). The overlapping regions (points 1 and 2) in figure 2(b) contribute to the high-dimensional two-photon path-entangled state, in which a pair of photons exists in the superposition of three states: both in mode 1, both in mode 2, and separated in modes 1 and 2. When the temperature continues to increase, $\vec{G}_{2,0}$ and $\vec{G}_{0,2}$ cannot compensate the phase mismatch and only one SPDC process supported by $\vec{G}_{1,1}$ exists, and the emission angles keep decreasing before the last SPDC process finally disappears.

Similarly, figures 3(b) and (c) give results from HPLT and 1D PPLT crystals, respectively. In figure 3(b), Point A corresponds to the situation when two conical beam are tangent and the heralded single-photon entangled state can be achieved, as illuminated in the lower of figure 1(b), while Point B gives the beam-like two-photon NOON state as shown in the upper of figure 1(b). After taking the thermal expansion of quadratic NPCs [33] into account, the theoretical (black line) and experimental (red dots) values agree well. Slight difference may result from the fabrication deviation of the quadratic NPC period and the measurement aberration in temperature.

2.4. Experimental measurement of photon flux of concurrent QPM-SPDC processes

The conversion efficiency of SPDC processes in quadratic NPCs is crucial for evaluating the potential as bright quantum light sources. We pump the crystal with a 532 nm CW laser whose power keeps 637 mW, and measure the photon flux by capturing down-converted photons with an EMCCD (Andor Solis iXon3 888) behind a 1064 nm interference filter of

40 nm bandwidth. Figures 3(d)–(f) show the total counts of down-converted photons in our RPLT, HPLT and 1D PPLT crystals, respectively. The measured conversion efficiency of SPDC process in 1D PPLT exhibits the highest one, being 9.54×10^{-9} pairs per pump photon, while efficiencies in 2D HPLT and RPLT turn out to be 7.63×10^{-9} and 1.17×10^{-9}, respectively (the length of crystals is 20 mm, 18 mm, 18 mm respectively). Consider the transmissivity of the interference filter is 61%, total conversion efficiency is 1.56×10^{-8}, 1.25×10^{-8}, and 1.93×10^{-9} respectively. Here for concurrent SPDC processes, we have summed up all the spatial modes.

Figure 3(d) shows how the photon flux of RPLT varies with the temperature. At a low temperature (point A), there exist three concurrent SPDC processes supported by $\vec{G}_{2,0}$, $\vec{G}_{0,2}$ and $\vec{G}_{1,1}$, respectively. As the temperature rises, the photon flux keeps constant within a range of temperature until point B, where only one SPDC process can be supported by $\vec{G}_{1,1}$, and the counts of down-converted photons decrease rapidly. When the temperature keeps increasing, $\vec{G}_{1,1}$ also fails to compensate the phase mismatch after point D. The photon flux of each SPDC process can be obtained and it should be decided by the Fourier coefficient of the involved reciprocal vector. Similarly, figures 3(e) and (f) give the results from HPLT and 1D PPLT crystals, respectively.

In our experiment, the pump beam waist radius is 59.5 μm, and only the down-converted photons whose emission angles outside the crystals are less than 7.75 mrad can overlap with the pump beam in the whole crystal. The walk-off length of down-converted photons is smaller than the length of crystals under most circumstances. We can see from figures 3(a) and (d) that the photon flux of concurrent SPDC processes does not decrease when the walk-off length is much smaller than the crystal length (when the temperature ranges from about 190 °C–220 °C).

3. Spatial correlation anisotropy of down-converted photons

3.1. Theoretical description of two-photon spatial correlation under concurrent noncollinear QPM-SPDC processes

Photonic quantum technology requires further understanding about the two-photon spatial correlation. When the pump beam is strongly focused, the photon pair generated through noncollinear phase-matching exhibit obvious spatial correlation asymmetry [34–36], which can influence correlation measurement and quantum imaging. However, the previous studies focus on single SPDC process fulfilled by a collinear reciprocal vector, where entangled photons distribute symmetrically beside the pump beam. The asymmetry in spatial correlation mainly results from both the noncollinear propagation of two photons and the birefringence of crystal. In this paper we focus on studying the spatial correlation of entangled photons generated by concurrent SPDC processes wherein multiple noncollinear reciprocal vectors are involved and the birefringence is smaller enough to be ignored. As an example, in the following discussion we will calculate the spatial correlation of photon pairs generated by the HPLT shown in figure 1(f).

The focused Gaussian pump beam can be treated as classical wave under paraxial propagation condition,

$$E_{\rm p}^{(+)}(\vec{\rho}, z, t) = E_0 \int {\rm d}\vec{q}_{\rm p} \exp\left(-\frac{q_{\rm p}^2\omega_0^2}{4}\right) \times \exp[{\rm i}(k_{{\rm p}z} z + \vec{q}_{\rm p}\cdot\vec{\rho} - \omega_{\rm p} t)], \quad (9)$$

while the signal and idler fields are treated quantum mechanically,

$$E_j^{(-)}(\vec{r}_j, t) = \int {\rm d}\vec{q}_j \exp[-{\rm i}(\vec{k}_j\cdot\vec{r}_j - \omega_j t)]\hat{a}^\dagger(\vec{q}_j). \quad (10)$$

Here we focus on the spatial correlation of two-photon state and treat three interactive waves as monochromatic ones with angular frequency of $\omega_{\rm p}$, $\omega_{\rm s}$ and $\omega_{\rm i}$, respectively, which could be experimentally justified by narrowband filters. ω_0 stands for the waist radius of pump beam. $\vec{k}_{\rm p}$ and $\vec{k}_j (j = s, i)$ are wave vectors of the three interacting waves. $k_{{\rm p}z}$ is the projection of $\vec{k}_{\rm p}$ in z direction. $\vec{q}_{\rm p}$ and $\vec{q}_j (j = s, i)$ are the transverse wave vectors of pump, signal and idler.

By taking equations (9) and (10) into (2), under the first order perturbation theory, the two-photon state can be expressed as

$$|\Psi\rangle = \psi_0 \iint {\rm d}\vec{q}_{\rm s1}{\rm d}\vec{q}_{\rm i1}\Phi(\vec{q}_{\rm s1}, \vec{q}_{\rm i1})\hat{a}^\dagger(\vec{q}_{\rm s1})\hat{a}^\dagger(\vec{q}_{\rm i1})|0\rangle + \psi_0 \iint {\rm d}\vec{q}_{\rm s2}{\rm d}\vec{q}_{\rm i2}\Phi(\vec{q}_{\rm s2}, \vec{q}_{\rm i2})\hat{a}^\dagger(\vec{q}_{\rm s2})\hat{a}^\dagger(\vec{q}_{\rm i2})|0\rangle, \quad (11)$$

in which $\Phi(\vec{q}_{\rm s1}, \vec{q}_{\rm i1})$ and $\Phi(\vec{q}_{\rm s2}, \vec{q}_{\rm i2})$ are two-photon mode functions ensured by $\vec{G}_{1,0}$ and $\vec{G}_{0,1}$, respectively. Due to the symmetry of the crystal, the two mode functions are the same, so we can simply concentrate on one mode when calculating the spatial correlation:

$$|\Psi\rangle_1 = \psi_0 \iint {\rm d}\vec{q}_{\rm s}{\rm d}\vec{q}_{\rm i}\Phi(\vec{q}_{\rm s}, \vec{q}_{\rm i})\hat{a}^\dagger(\vec{q}_{\rm s})\hat{a}^\dagger(\vec{q}_{\rm i})|0\rangle \quad (12)$$

in which the two-photon mode function can be written as

$$\Phi(\vec{q}_{\rm s}, \vec{q}_{\rm i}) = E(\vec{q}_{\rm s}, \vec{q}_{\rm i}){\rm sinc}(\Delta k_z L/2). \quad (13)$$

Here we have considered that the cross section of the crystal is much larger than the interaction region of three waves, so it can be treated as infinity. $E(\vec{q}_{\rm s}, \vec{q}_{\rm i})$ is introduced by the focused pump, and $\Delta k_z = k_{{\rm p}z} - k_{{\rm s}z} - k_{{\rm i}z} - G_z$ is the phase mismatch along z axis, i.e. the propagation direction of the pump. G_z is the projection of reciprocal vector $\vec{G}_{1,0}$ (or $\vec{G}_{0,1}$) in z direction, and $k_{jz} = k_{j{\rm L}}\cos\theta_j - q_{j\|}\sin\theta_j$ $(j = s, i)$ is the projection of k_j along z direction. $k_{j{\rm L}} = \sqrt{k_j^2 - q_j^2}$ is the longitudinal wave vector of entangled photons which has a noncollinear angle θ_j with the z axis in noncollinear geometries. The transverse wave vector $\vec{q}_j$ contains in-plane (x–z plane) and out-of-plane projections, written as $q_{j\|}$ and $q_{j\perp}$ in turn, where $q_j = \sqrt{q_{j\|}^2 + q_{j\perp}^2}$. Using the first order Taylor

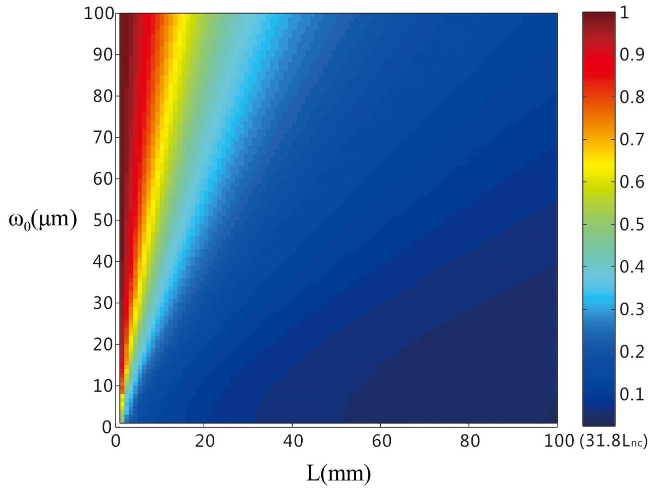

Figure 4. The theoretical calculation of the dependence of parameter η on crystal length L and pump beam waist ω_0.

expansion we can get

$$E(\vec{q}_s, \vec{q}_i) = \exp\left\{-\left[\left(q_{s\parallel}\cos\theta_s + q_{i\parallel}\cos\theta_i - \frac{q_s^2}{2k_s}\sin\theta_s - \frac{q_i^2}{2k_i}\sin\theta_i\right)^2 + (q_{s\perp} + q_{i\perp})^2\right]\frac{\omega_0^2}{4}\right\}, \tag{14}$$

$$\Delta k_z = -\frac{\left(q_{s\parallel}\cos\theta_s + q_{i\parallel}\cos\theta_i - \frac{q_s^2}{2k_s}\sin\theta_s - \frac{q_i^2}{2k_i}\sin\theta_i\right)^2}{2k_p} - \frac{(q_{s\perp} + q_{i\perp})^2}{2k_p} + \frac{q_s^2\cos\theta_s}{2k_s} + \frac{q_i^2\cos\theta_i}{2k_i} + q_{s\parallel}\sin\theta_s + q_{i\parallel}\sin\theta_i. \tag{15}$$

Compared with the SPDC process in collinear geometry [37], we can see that noncollinear QPM introduces extra terms, thus resulting in the asymmetry between $q_{j\parallel}$ and $q_{j\perp}$.

In collinear SPDC geometry, $\theta_s = \theta_i = 0$, equations (14) and (15) write

$$E(\vec{q}_s, \vec{q}_i) = \exp\left(-[(q_{s\parallel} + q_{i\parallel})^2 + (q_{s\perp} + q_{i\perp})^2]\frac{\omega_0^2}{4}\right), \tag{16}$$

$$\Delta k_z = -\frac{(q_{s\parallel} + q_{i\parallel})^2}{2k_p} - \frac{(q_{s\perp} + q_{i\perp})^2}{2k_p} + \frac{q_s^2}{2k_s} + \frac{q_i^2}{2k_i}. \tag{17}$$

Similar results have been reported in [38–40].

Experimentally, we keep detecting the idler photon at the center of the Fourier plane of a lens where $q_{i\parallel} = q_{i\perp} = 0$, and scan the other detector for the signal photon to study the asymmetry of spatial correlation in and out of x–z plane. In our experimental setup, $|\vec{q}_j|$ is small compared with wave vector $|\vec{k}_j|$, and $\sin\theta_j \ll 1$. So we get a simplified form of in-plane and out-of-plane mode function.

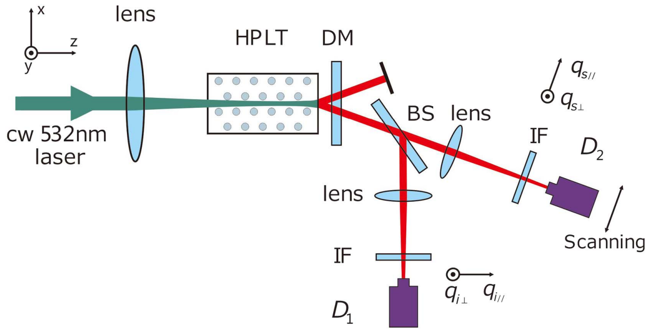

Figure 5. Experimental setup for spatial correlation ellipticity measurement. The HPLT crystal is controlled at 172.3 °C and pumped with a 532 nm laser to generate the two-photon NOON state. The waist of pump beam is 59.5 μm, and the length of crystal is 18 mm. After the crystal, the down-converted photons of 1064 nm are separated from the pump by a dichromatic mirror. Then one mode of the NOON state is blocked, while the other mode is split into two beams and detected by two single photon detectors at the Fourier planes of two lenses for 2D coincidence counting measurement. The bandwidth of 1064 nm interference filter is 10 nm, and the detector for the signal has a 80 × 80 μm^2 sensing area, scanned in the Fourier plane of a $f = 38.1$ mm lens, and the detector for the idler has a sensing area of 180 × 180 μm^2, centered at the Fourier plane of a $f = 50$ mm lens.

When $q_{s\perp} = 0$, we get the in-plane correlation

$$\Phi(q_{s\parallel}, 0, 0, 0) = \exp\left[-\left(\frac{q_{s\parallel}\omega_0\cos\theta_s}{2}\right)^2\right] \times \mathrm{sinc}\left[\left(-\frac{q_{s\parallel}^2\cos^2\theta_s}{2k_p} + \frac{q_{s\parallel}^2\cos\theta_s}{2k_s} + q_{s\parallel}\sin\theta_s\right)\frac{L}{2}\right]$$
$$= \exp\left[-\left(\frac{q_{s\parallel}\omega_0\cos\theta_s}{2}\right)^2\right] \times \mathrm{sinc}\left[-\left(\frac{q_{s\parallel}\omega_0\cos\theta_s}{2}\right)^2\xi + \left(\frac{q_{s\parallel}\omega_0}{2}\right)^2 \times \frac{\cos\theta_s k_p}{k_s}\xi + \left(\frac{q_{s\parallel}\omega_0}{2}\right)\frac{L}{L_{nc}}\right]. \tag{18}$$

Meanwhile, when $q_{s\parallel} = 0$, we get the out-of-plane correlation

$$\Phi(0, q_{s\perp}, 0, 0) = \exp\left[-\left(\frac{q_{s\perp}\omega_0}{2}\right)^2\right] \times \mathrm{sinc}\left[\left(-\frac{q_{s\perp}^2}{2k_p} + \frac{q_{s\perp}^2\cos\theta_s}{2k_s}\right)\frac{L}{2}\right]$$
$$= \exp\left[-\left(\frac{q_{s\perp}\omega_0}{2}\right)^2\right]\mathrm{sinc}\left[-\left(\frac{q_{s\perp}\omega_0}{2}\right)^2\xi + \left(\frac{q_{s\perp}\omega_0}{2}\right)^2\frac{\cos\theta_s k_p}{k_s}\xi\right]. \tag{19}$$

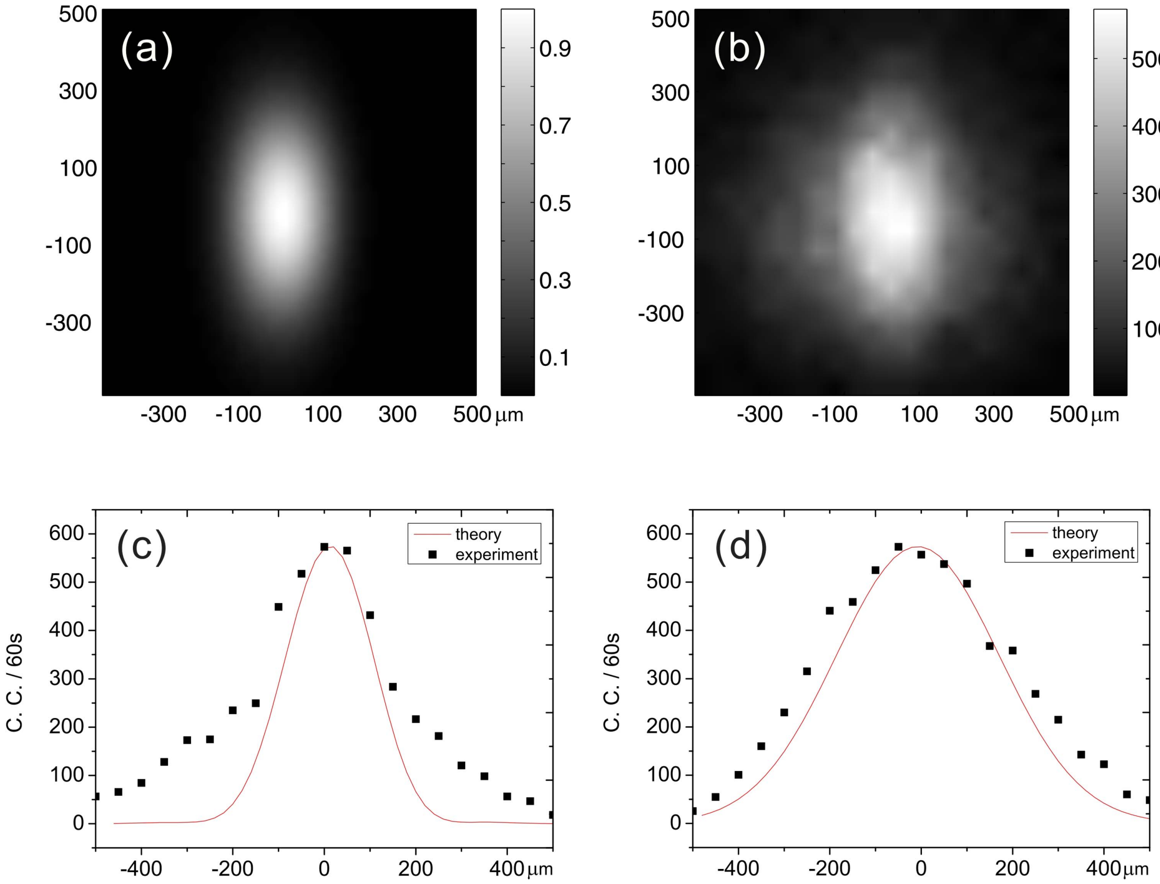

Figure 6. (a) Theoretical and (b) experimental results of the two-photon spatial correlation in one mode of two-photon NOON state. (c) The extracted spatial correlation in x–z plane and (d) y direction, black dots stand for measured data, and the red lines show the theoretical calculation.

In which $L_{\mathrm{nc}} = \omega_0 / \sin\theta_{\mathrm{s}}$ represents the noncollinear length, which describes the noncollinear geometry [35] and $\xi = L/k_{\mathrm{p}}\omega_0^2$ is the focus parameter of the pump beam.

From equations (18) and (19) we find that the in-plane spatial correlation is both decided by ξ and L_{nc}, while the out-of-plane correlation only depends on ξ. If $L \ll L_{\mathrm{nc}}$, equations (18) and (19) exhibit nearly the same spatial correlation. However, if $L \sim L_{\mathrm{nc}}$, the spatial correlation along two directions differ from each other, thus exhibiting spatial anisotropy.

We define a parameter $\eta = \Delta q_{j\|}/\Delta q_{j\perp}$ to describe the anisotropy, where $\Delta q_{j\|}$, $\Delta q_{j\perp}$ represent the full width at half maximum of spatial correlation along direction of $q_{j\|}$ and $q_{j\perp}$. When $\eta \doteq 1$, spatial correlation appears to be symmetrical, otherwise, small η indicates explicit spatial anisotropy. Figure 4 is the theoretical simulation of how η varies with ω_0 and L under the QPM situation illuminated by the upper of figure 1(b). The spatial correlation tends to be asymmetrical when the pump beam is strongly focused in long quadratic NPCs. Furthermore, as concurrent SPDC processes provide possibilities for flexible spatial mode modulation, correlation asymmetrical can be easily altered through noncollinear QPM geometry engineering.

3.2. Experimental measurement of spatial correlation under noncollinear QPM geometry

In this section, we experimentally observe the spatial correlation ellipticity in the noncollinear QPM geometry. Figure 5 shows the experimental setup. The HPLT crystal works in the noncollinear QPM geometry shown in the upper of figure 1(b), which generate the two-photon NOON state [14], and only one mode of the NOON state is used to measure the ellipticity of spatial correlation while the other is blocked. We fix one single photon detector at the center of Fourier plane behind the HPLT crystal, and scan the other detector at the Fourier plane to perform 2D coincidence measurements. Figure 6(a) illustrates the theoretically simulation of the 2D spatial correlation and figure 6(b) shows the experimental results. The horizontal and vertical axises are along directions of $q_{j\|}$ and $q_{j\perp}$, respectively. Figures 6(c) and (d) demonstrate the extracted spatial correlation in and out of the x–z plane which are expressed by equations (18) and (19), both theoretically and experimentally. The influence of detector diameter has been taken into consideration. The length of HPLT crystal is 18 mm and the waist radius of pump beam is 59.5 μm, giving the expectation of η for NOON state to be 0.410. And the measurement gives $\eta = 0.594$, exhibiting obvious asymmetry in spatial correlation as well. The deviation between experimental measurement and theoretical expectation may be induced by temperature fluctuation and the photon pairs with nondegenerate wavelengths, which were also detected in our experiment due to the finite bandwidth of interference filters. To meet the QPM condition, photon pairs with nondegenerate wavelengths should exhibit conical modes, resulting in the expansion of spatial correlation. And the narrower spatial correlation in x–z plane is more susceptible to the expansion.

4. Discussion

We reported our exploration about concurrent SPDC processes in 2D domain-engineered NPCs. The detailed characterization on the performance of concurrent SPDC processes will give valuable references to the construction of compact path entanglement. When introducing more functions into the NPC, such as beam splitting and focusing [25], it will become an attractive element in prompting the development of photonic quantum technologies.

Acknowledgments

This work was supported by the National Natural Science Foundation of China (Contracts No. 11422438, No. 11690031, No. 11627810 and No. 11621091).

References

[1] O'Brien J L, Furusawa A and Vučković J 2009 *Nat. Photon.* **3** 687–95
[2] Politi A, Matthews J C F, Thompson M G and O'Brien J L 2009 *IEEE J. Sel. Top. Quantum Electron.* **15** 1673–84
[3] Berger V 1998 *Phys. Rev. Lett.* **81** 4136–9
[4] Broderick N G R, Ross G W, Offerhaus H L, Richardson D J and Hanna D C 2000 *Phys. Rev. Lett.* **84** 4345–8
[5] Xu P and Zhu S N 2012 *AIP Adv.* **2** 041401
[6] Gallo K, Levenius M, Laurell F and Pasiskevicius V 2011 *App. Phys. Lett.* **98** 161113
[7] Chen L, Xu P, Bai Y F, Luo X W, Zhong M L, Dai M, Lu M H and Zhu S N 2014 *Opt. Express* **22** 13164–9
[8] Levenius M, Pasiskevicius V and Gallo K 2012 *Appl. Phys. Lett.* **101** 121114
[9] Lazoul M, Boudrioua A, Simohamed L M and Peng L H 2015 *Opt. Lett.* **40** 1861–4
[10] Lazoul M, Boudrioua A, Simohamed L M, Fischer A and Peng L H 2013 *Opt. Lett.* **38** 3892–4
[11] Liu H C and Kung A H 2008 *Opt. Express* **16** 9714–25
[12] Gong Y X, Xu P, Bai Y F, Yang J, Leng H Y, Xie Z D and Zhu S N 2012 *Phys. Rev.* A **86** 023835
[13] Megidish E, Halevy A, Eisenberg H S, Ganany-Padowicz A, Habshoosh N and Arie A 2013 *Opt. Express* **21** 6689–96
[14] Jin H, Xu P, Luo X W, Leng H Y, Gong Y X, Yu W J, Zhong M L, Zhao G and Zhu S N 2013 *Phys. Rev. Lett.* **111** 023603
[15] Pelton M, Marsden P, Ljunggren D, Tengner M, Karlsson A, Fragemann A, Canalias C and Laurell F 2004 *Opt. Express* **12** 3573–80
[16] Kuklewicz C E, Fiorentino M, Messin G, Wong F N C and Shapiro J H 2004 *Phys. Rev.* A **69** 013807
[17] Fedrizzi A, Herbst T, Poppe A, Jennewein T and Zeilinger A 2007 *Opt. Express* **15** 15377–86
[18] Lee S M, Kim H, Cha M and Moon H S 2016 *Opt. Express* **24** 2941–53
[19] Bharadwaj D and Thyagarajan K 2016 *Phys. Rev.* A **94** 063816
[20] Giovannetti V, Maccone L, Shapiro J H and Wong F N C 2002 *Phys. Rev. Lett.* **88** 183602
[21] Kuzucu O, Fiorentino M, Albota M A, Wong F N C and Kaertner F X 2005 *Phys. Rev. Lett.* **94** 083601
[22] Nasr M B, Carrasco S, Saleh B E A, Sergienko A V, Teich M C, Torres J P, Torner L, Hum D S and Fejer M M 2008 *Phys. Rev. Lett.* **100** 183601
[23] Kim H, Lee H J, Lee S M and Moon H S 2015 *Opt. Lett.* **40** 3061–4
[24] Yu X Q, Xu P, Xie Z D, Wang J F, Leng H Y, Zhao J S, Zhu S N and Ming N B 2008 *Phys. Rev. Lett.* **101** 233601
[25] Leng H Y, Yu X Q, Gong Y X, Xu P, Xie Z D, Jin H, Zhang C and Zhu S N 2011 *Nat. Commun.* **2** 429
[26] Torres J P, Alexandrescu A, Carrasco S and Torner L 2004 *Opt. Lett.* **29** 376–8
[27] Shi B S, Wang F Y, Zhai C and Guo G C 2008 *Opt. Commun.* **281** 3390–4
[28] Lu L L, Xu P, Zhong M L, Bai Y F and Zhu S N 2015 *Opt. Express* **23** 1203–12
[29] Hiesmayr B C, de Dood M J A and Löffler W 2016 *Phys. Rev. Lett.* **116** 073601
[30] Miatto F M, Yao A M and Barnett S M 2011 *Phys. Rev.* A **83** 033816
[31] Rubin M H 1996 *Phys. Rev.* A **54** 5349–60
[32] Meyn J P and Fejer M M 1997 *Opt. Lett.* **22** 1214–6
[33] Bruner A, Eger D, Oron M B, Blau P, Katz M and Ruschin S 2003 *Opt. Lett.* **28** 194–6
[34] Molina-Terriza G, Minardi S, Deyanova Y, Osorio C I, Hendrych M and Torres J P 2005 *Phys. Rev.* A **72** 065802
[35] Torres J P, Molina-Terriza G and Torner L 2005 *J. Opt. B: Quantum Semiclass. Opt.* **7** 235–9
[36] Fedorov M V, Efremov M A, Volkov P A, Moreva E V, Straupe S S and Kulik S P 2007 *Phys. Rev. Lett.* **99** 063901
[37] Yun S J, Xu P, Zhao J S, Gong Y X, Bai Y F, Shi J and Zhu S N 2012 *Phys. Rev.* A **86** 023852
[38] Monken C H, Souto Ribeiro P H and Pádua S 1998 *Phys. Rev.* A **57** 3123–6
[39] Walborn S P and Monken C H 2007 *Phys. Rev.* A **76** 062305
[40] Grice W P, Bennink R S, Goodman D S and Ryan A T 2011 *Phys. Rev.* A **83** 023810